RSC Advances

PAPER

View Article Online
View Journal | View Issue

Cite this: *RSC Adv.*, 2016, **6**, 47520

Synthesis and *in vitro* cytotoxicity evaluation of ruthenium polypyridyl-sensitized paramagnetic titania nanoparticles for photodynamic therapy†

Mohammad H. Sakr,[a] Najeeb M. Halabi,‡[b] Leen N. Kalash,[a] Sara I. Al-Ghadban,[b] Mayyasa K. Rammah,§[b] Marwan E. El Sabban,*[b] Kamal H. Bouhadir*[a] and Tarek H. Ghaddar*[a]

Magnetite/silica/titania core–shell–shell nanoparticles were synthesized by sol–gel methods and characterized by various methods. The hydrodynamic radius of the final nanoparticle sample was measured by dynamic light scattering and found to be 99 nm. Following hydrothermal treatment of the final nanocomposites, a ruthenium polypyridyl dye was anchored to the surface. The total potential reactive oxygen species (ROS) generation and singlet oxygen ($^1O_2$) production in solution by the hybrid NPs (naked NPs + ruthenium dye) were evaluated by fluorescence and UV-Vis spectroscopy. Under 532 nm light illumination, more than a five-fold increase in ROS production was observed with the hybrid NPs in comparison to the bare NPs or the ruthenium dye alone. Similar results were obtained under white light illumination as well. Moreover, singlet oxygen generation produced by the hybrid NPs was found to be negligible. The photodynamic effect of the excited NPs on the viability of lung cancer cells (A549) was evaluated *in vitro*. ROS production in A549 NP-loaded cells was measured and a live/dead cell assay was conducted. There was a significant, light excitation-dependent increase in ROS production and induction of cell death in light excited A549 NP-loaded cells as compared to control cells and NP loaded cells without excitation. These findings demonstrate that the hybrid NPs can potentially act as type I photodynamic therapy (PDT) agents generating free radicals, unlike the currently employed ones in medicine which follow a type II mechanism predominantly (generating singlet oxygen). This type of photosensitizers can prove advantageous in eradicating PDT-resilient hypoxic tumors, avoiding type II photosensitizers-induced hypoxia in non-hypoxic tumor cells.

Received 14th April 2016
Accepted 5th May 2016

DOI: 10.1039/c6ra09696d

www.rsc.org/advances

Introduction

Photodynamic therapy (PDT) is a minimally invasive treatment modality of various diseases, especially early and localized tumors, where malignant cells are destroyed by light-induced generation of reactive oxygen species (ROS).[1] ROS production generally commences with photosensitizers administered topically or systemically.[2] Illuminating the targeted tissue initiates oxidative damage through radiation-induced apoptosis, necrosis, or autophagy.[3] PDT is mediated by either a type I mechanism involving the production of free radicals resulting from the activated sensitizer reacting with the plasma membrane or other intracellular moieties; or by a type II mechanism that involves generation of singlet oxygen ($^1O_2$) upon energy transfer from the activated sensitizer to oxygen.[2]

Historically, most photosensitizers belong to one of the three families: porphyrins, chlorophylls, and phthalocyanines dyes.[4] It is commonly accepted that all photosensitizers follow a type II mechanism in their mode of action in PDT either exclusively or preferentially.[5] Ruthenium(II) polypyridyl complexes are one of the emerging families of photosensitizers that have shown efficient $^1O_2$ generation due to their relatively long lived triplet metal-to-ligand charge transfer excited states.[6] These complexes are known for their high photostability and synthetic tailorability for nonlinear optical properties (potential two-photon absorption in the spectral window of relative transparency of the biological media, 600–1000 nm).[7,8] Ruthenium complexes were generally evaluated for their antitumor activities greatly due to their ability to intercalate double-stranded DNA and RNA.[9,10] However, the application of ruthenium complexes as photosensitizers has only recently been exploited and most studies focused on conjugating these complexes to

[a]*Department of Chemistry, Faculty of Arts and Sciences, American University of Beirut, Lebanon. E-mail: tarek.ghaddar@aub.edu.lb; kbh05@aub.edu.lb*

[b]*Department of Anatomy, Cell Biology and Physiological Sciences, Faculty of Medicine, American University of Beirut, Lebanon. E-mail: me00@aub.edu.lb*

† Electronic supplementary information (ESI) available. See DOI: 10.1039/c6ra09696d

‡ Current address: Department of Genetic Medicine, Weill Cornell Medical College, Qatar.

§ Current address: Aix-Marseille University, Developmental Biology Institute of Marseille, CNRS UMR7288, France.

conventional photosensitizers, such as porphyrins, which is advantageous in enhancing light absorption, cellular uptake, quantum yield, and, most importantly, cytotoxicity.[11–21] Although the antitumor activity of these hybrids is enhanced compared to the individual components, these approaches require lengthy synthesis pathways and cumbersome purification steps.

In recent years, there have been multiple reports on the use of ruthenium polypyridyl complexes as photosensitizers in PDT,[7,8,22,23] where cytotoxicity in all cases was attributed to the formation of $^1O_2$ from molecular oxygen. Consequently, tissue oxygenation plays a major role in determining the effectiveness of singlet oxygen-mediated (type II) PDT outcome, and in case of molecular oxygen deficiency during irradiation of this type of photosensitizers, the photo-treatment will have little to no antitumor cell effect. In fact, it's known that hypoxic (poorly oxygenated) tumors cells are generally resistant to PDT, in addition to radiotherapy and chemotherapy.[24] There are two types of hypoxia: (1) pre-existing hypoxic cells, which are a result of tumor physiological development and exist in many solid tumors; (2) the PDT itself can also induce acute hypoxia due to fast depletion of local oxygen supply.[25] Therefore, the development of photosensitizers that can generate free radicals instead, exclusively or preferentially, is clearly advantageous not only for hypoxic tumors, but also for all types of malignant cells.

A variety of photosensitizers have been developed thus far, however, only a dozen are approved for clinical use.[4] Some of the encountered limitations include poor selectivity resulting in the damage of healthy tissues, high hydrophobicity preventing intravenous administration and lowering quantum yields due to aggregation and finally, prolonged skin accumulation causing hypersensitivity to sun exposure for up to weeks after a common treatment. Overcoming these problems is a major challenge in the development of effective PDT sensitizers.[2,3,5] To overcome some of these limitations, recent efforts focused on coupling organic photosensitizers to macromolecular drug carriers. Among these, inorganic nanoparticles (NPs) hold a great promise due to some intrinsic properties such as stability (in pH changes, and against microbial attack and enzymatic degradation), synthetic control over shape, size, and porosity. In addition, inorganic nanoparticles (1) could be made hydrophilic, (2) their high surface area can be functionalized to achieve various biochemical and tumor targeting purposes, (3) they can be readily taken up and effectively retained in tumor cells due to the enhanced permeability and retention effect (EPR) of the latter, (4) they can be made to serve multiple purposes such as MRI contrast agents by incorporating a magnetic core, in addition to actively participating in the photo-physical action of the attached photosensitizer in PDT, or in combinational therapy.[1,2,26]

Titanium dioxide (TiO_2) is a wide band gap semiconductor that is known for its high photosensitivity. Upon irradiation with ultraviolet light A (UVA) below 385 nm, electrons are exited into the conduction band, leaving positive holes in the valence band. Both of these charge carriers react with surrounding water and molecular oxygen to yield various ROS species.[27] TiO_2 was first reported to photo-kill malignant cells by Fujishima *et al.*[28] Since then, there has been a growing interest in the use of TiO_2 NPs as photosensitizers in PDT.[29–35] In order to enhance their dispersion, cell compatibility, and cytotoxicity various research groups resorted to surface modification of these NPs with different organic and inorganic compounds.[36–42] However, a major limitation for the use of TiO_2 *in vivo* was its photo-excitation by UVA only, which has a limited penetration depth of a few millimeters in human tissue, and is mostly absorbed by surrounding tissue. Several methods were developed to extend the optical absorption of TiO_2 NPs to the visible spectrum. Doping[43–49] and sensitization[50–55] are the most extensively applied approaches in TiO_2-mediated PDT.[54] Recently, Tokuoka *et al.* attached an FDA approved porphyrin photosensitizer, chlorin e6, to TiO_2 NPs. Irradiation of polychromatic light (550–750 nm), that excites chlorin e6, significantly damaged murine lymphoma cell line (EL-4 cells) and a higher cell-killing effect was found for the dye-TiO_2 particles than for the system using chlorin e6 alone.[50] Lopez *et al.* incorporated an efficient photosensitizer, zinc phthalocyanine (ZnPc) molecules, into the porous network of TiO_2 using the sol–gel method. However, the photodynamic effect of the composite TiO_2–ZnPc on tumor and non-malignant mammalian cells was less potent than that of pure ZnPc alone.[52]

In this report we set to develop ruthenium polypyridyl sensitized titania-based hybrid NPs that follow type I PDT mechanism exclusively. To that end, core–shell–shell magnetite–silica–titania nanoparticles Fe_3O_4@SiO_2@TiO_2 (C-NPs) were synthesized by successive sol–gel methods, Scheme 1. The super-paramagnetic magnetite cores can be used as contrast agents for MRI as previously mentioned, and with the application of an external magnetic field at the tumor site, their

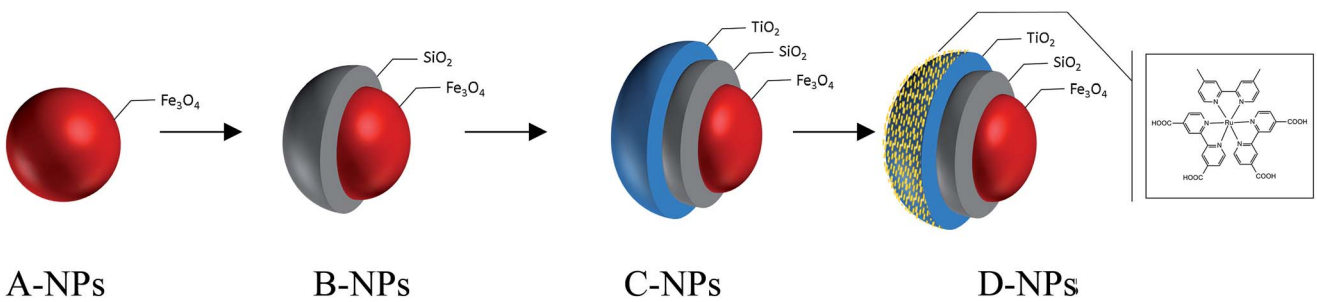

Scheme 1 Schematic representation of A, B, C and D nanoparticles.

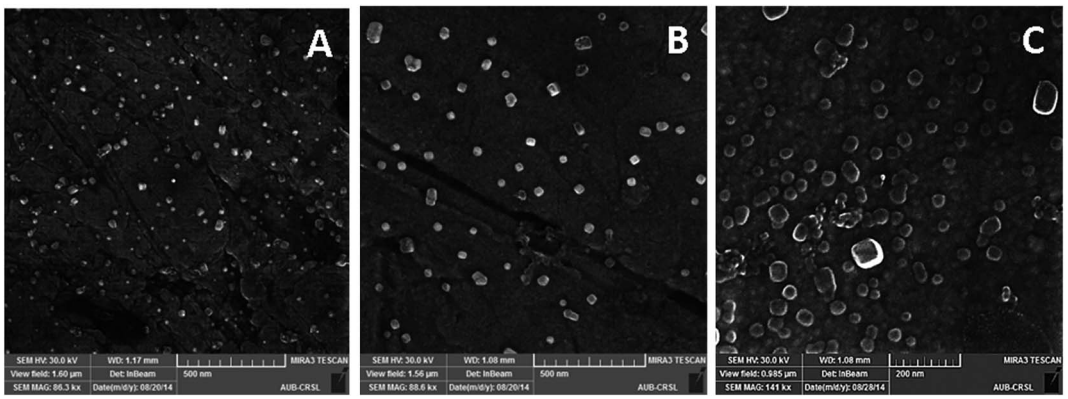

Fig. 1 SEM images of the different nanoparticles A-NPs, B-NPs and C-NPs.

accumulation and retention in the target tissue could be greatly enhanced. Next, a ruthenium dye, $[(4,4'\text{-dcbpy})_2\text{Ru(dm-bpy)}]\cdot 2\text{Cl}$ (where dc = dicarboxy, dm = dimethyl, and bpy = 2,2′-bipyridine), was anchored to the nanoparticles forming the hybrid photosensitizer $Fe_3O_4@SiO_2@TiO_2@$dye (D-NPs). The role of titania, is to accept the electron injected from the photo-excited dye into its conduction band (similar to how a dye sensitized solar cell work). Theoretically, both holes in the oxidized dye and accumulated electrons in TiO_2 can oxidize and reduce, respectively, surrounding species (especially oxygen and water) to form cytotoxic free radicals (PDT type I). The silica buffer layer between magnetite and titania acts as an insulating layer preventing electron–hole recombination at the magnetite center, thus increasing the lifetime of the photo-generated holes (at the dye end) and electrons (at the titania end), and hence their photo-reactivity.[56]

In this study, we demonstrate the effective cytotoxic properties of this novel composition of NPs in an *in vitro* model of human lung cancer cell line (A549 cells). To our knowledge, this is the first report on the use of ruthenium complex-sensitized metal oxides in PDT, where type I mechanism is realized exclusively.

Table 1 Mean diameters of the different NPs obtained by SEM and DLS

Sample	SEM mean equivalent diameter (nm)	DLS intensity-weighed hydrodynamic diameter (nm)
A-NPs	17	62
B-NPs	27	90
C-NPs	40	99

Material and methods

Instruments and equipment

X-ray diffraction measurements were performed using Bruker D8 Discover. Fourier transform infrared (FT-IR) spectra were collected on Nicolet 4700, Thermo Electron Corporation. The surface areas of the different samples were calculated according to Brunauer–Emmet–Teller (BET) model from nitrogen adsorption isotherms carried out on Nova 2200e Surface Area and Pore Size Analyzer, Quantachrome Instruments. Energy-dispersive X-ray spectroscopy (EDX) spectra and scanning electron microscopy (SEM) images of the nanoparticles were obtained using Tescan Mira 3 MLU, and X-Max Silicon drift detector with 20 mm^2-detector size, Oxford Instruments. The

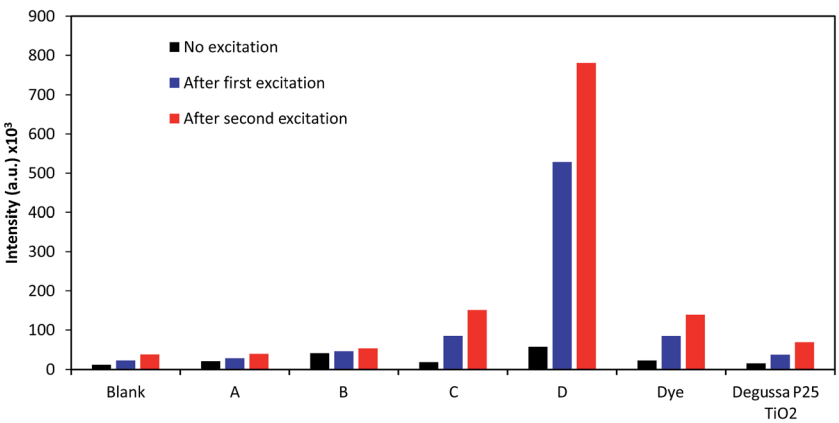

Fig. 2 Fluorescence intensities of DCF at 520 nm after successive 532 nm excitation (5 min intervals) of the blank control, A-NPs, B-NPs, C-NPs, D-NPs, dye, and Degussa P25 TiO_2 NPs. Excitation intervals were separated by a 5 min in-dark intervals.

hydrodynamic radii of the NPs were measured using 90Plus Particle Size Analyzer, Brookhaven Instruments Corporation. Total ROS and singlet oxygen generations were assessed by measuring the emission of a fluorescent probe using Fluorolog FL-1057 from Horiba Jobin Yvon, and the UV-Vis spectra of another probe using Jasco V-570, respectively. Images of excitation and viability of A549 cells were captured with two channels, 488 nm (calcein) and 561 nm (PI) using LSM710 confocal microscope (Zeiss, Germany). In the case of ROS production, images were captured immediately after excitation at 520 nm (DHE). The excitation light for both solution and cell ROS measurements were: a white light source (halogen lamp 50 mW cm^{-2} equipped with a UV filter <350 nm) or a monochromatic 532 nm light (laser diode 5 mW cm^{-2}).

Materials

Iron(II) chloride tetrahydrate ($FeCl_2 \cdot 4H_2O$) (99%), iron(III) chloride hexahydrate ($FeCl_3 \cdot 6H_2O$) (97%), propidium iodide (PI), and fluorescein isothiocyanate were purchased from Sigma-Aldrich. Tetraethyl orthosilicate (TEOS) ($C_8H_{20}O_4Si$) (99%), poly(acrylic acid, sodium salt) $-(C_3H_3NaO_2)_n$ ($M_w \approx$ 2100), 9,10-dimethylanthracene (DMA), and 3-hydroxytyramine hydrobromide were obtained from Aldrich. Titanium(IV) isopropoxide ($C_{12}H_{28}O_4Ti$) (98%) was purchased from Acros Organics and Degussa P25 titania from Sigma-Aldrich. Sodium phosphate monobasic ($NaHPO_4 \cdot H_2O$) from Fisher Scientific Company and sodium phosphate, dibasic, anhydrous (Na_2PO_4) from Solar Laboratories, Inc. were used to make phosphate buffer solutions. 2,7-Dichlorodihydrofluorescein diacetate (DCFH-DA) was purchased from Cayman Chemical Company. Dihydroethidium (DHE), calcein-AM, and calcein-blue AM were purchased from life technologies. Glass Bottom Culture Dishes (Confocal dishes) were purchased from Matek® (USA), glass bottom 8 well chambers from BD falcon-USA. For cell culture, DMEM AQ culture media, penicillin G, streptomycin, fetal bovine serum and sodium pyruvate were ordered from Sigma-Aldrich. Solvents, and other chemicals, were of analytical grade and used without further purification. Distilled and deionized water was used throughout the work.

Nanoparticles preparation

The methods can be found in the ESI.†

Total ROS generation in solution

To quantify the ROS generated by D-NPs in solution, a PBS, 0.1 M, was prepared, and a solution of dichlorofluorescein (DCFH), 3.5 mM, was reconstituted by dissolving DCFH-DA in 10 mM NaOH. Next, 3 ml of PBS and 10 μl of DCFH were transferred into a quartz cuvette. Finally, 0.5 mg of various NP solutions (A-NPs, B-NPs, C-NPs, D-NPs, Deguassa P25 TiO_2 NPs) was added. The solution inside the cuvette was then exposed to either 532 nm monochromatic or white light while bubbling it with air to ensure oxygen saturation, and the emission spectrum ($\lambda_{ex} = 500$ nm, $\lambda_{em} = 520$ nm) was recorded at different intervals with light being on for 5 min and off for another 5.

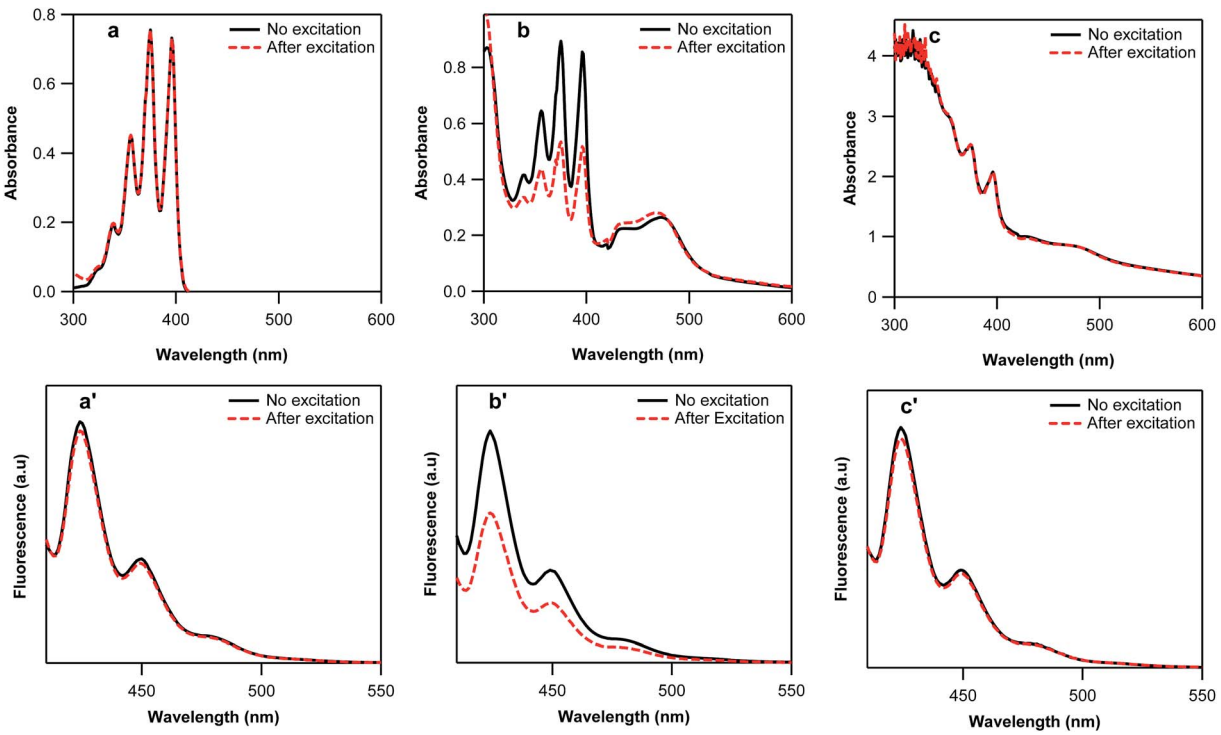

Fig. 3 UV-Vis (top) and fluorescence emission spectra (bottom) of DMA before and after 80 min excitation with a 532 nm light for the samples (a and a′) (blanks), (b and b′) (dye) and (c and c′) (D-NPs) in PBS buffer.

Singlet oxygen generation in solution

Singlet oxygen generation was measured using DMA as a probe. Two solutions were prepared: the first contains 7.5×10^{-5} M DMA and 1.5×10^{-5} M of dye, and another one having the same concentration of DMA plus 0.408 mg of D-NPs. UV-Vis and emission spectra ($\lambda_{ex} = 397$ nm) were recorded at $t = 0$ (immediately upon adding dye or D-NPs) and after 80 min of excitation with a 532 nm monochromatic light. A stream of air was bubbled into the solution throughout the experiment.

Quantifying dye anchored to D-NPs

The ruthenium complex was desorbed from D-NPs with the addition of aqueous NaOH. The mixture was centrifuged and the supernatant isolated. The UV-Vis spectrum of the supernatant was measured. The concentration of the free dye in solution was determined spectrophotometrically by measuring the UV-Vis absorption. The amount of the anchored dye to the NPs was calculated be 50 mmol g^{-1} of NPs ($\varepsilon_{475\ nm} \approx 17\ 000\ l\ mol^{-1}\ cm^{-1}$).

Cell culture

A549 cells, a human lung adenocarcinoma epithelial cell line, were grown in DMEM AQ culture media supplemented with penicillin G 100 U ml^{-1} and streptomycin 100 μg ml^{-1}, 10% Fetal Bovine Serum (FBS) and sodium pyruvate. Cells were cultured in a 37 °C incubator with 5% CO_2 atmosphere.

Excitation and viability measurements of A549 cells

A549 cells were seeded in glass bottom 8 well chambers (5000 cells per well). After 24 h, cells were loaded with D-NPs or left unloaded. For treatment, D-NPs were suspended in 95% ethanol and adjusted to 1 mg ml^{-1}. A solution of 1% v/v was added to 1 ml of media resulting in a concentration of 10 μg ml^{-1}. After 24 h of incubation, cells were washed to remove un-internalized D-NPs and incubated with propidium iodide (PI) at a concentration of 1 μg ml^{-1}. Propidium iodide (PI) is a membrane impermeable dye that intercalates with nucleic acids. If cell viability is compromised, membrane integrity is lost, and PI can then enter cells, bind DNA and become fluorescent. Following PI addition, one 8-

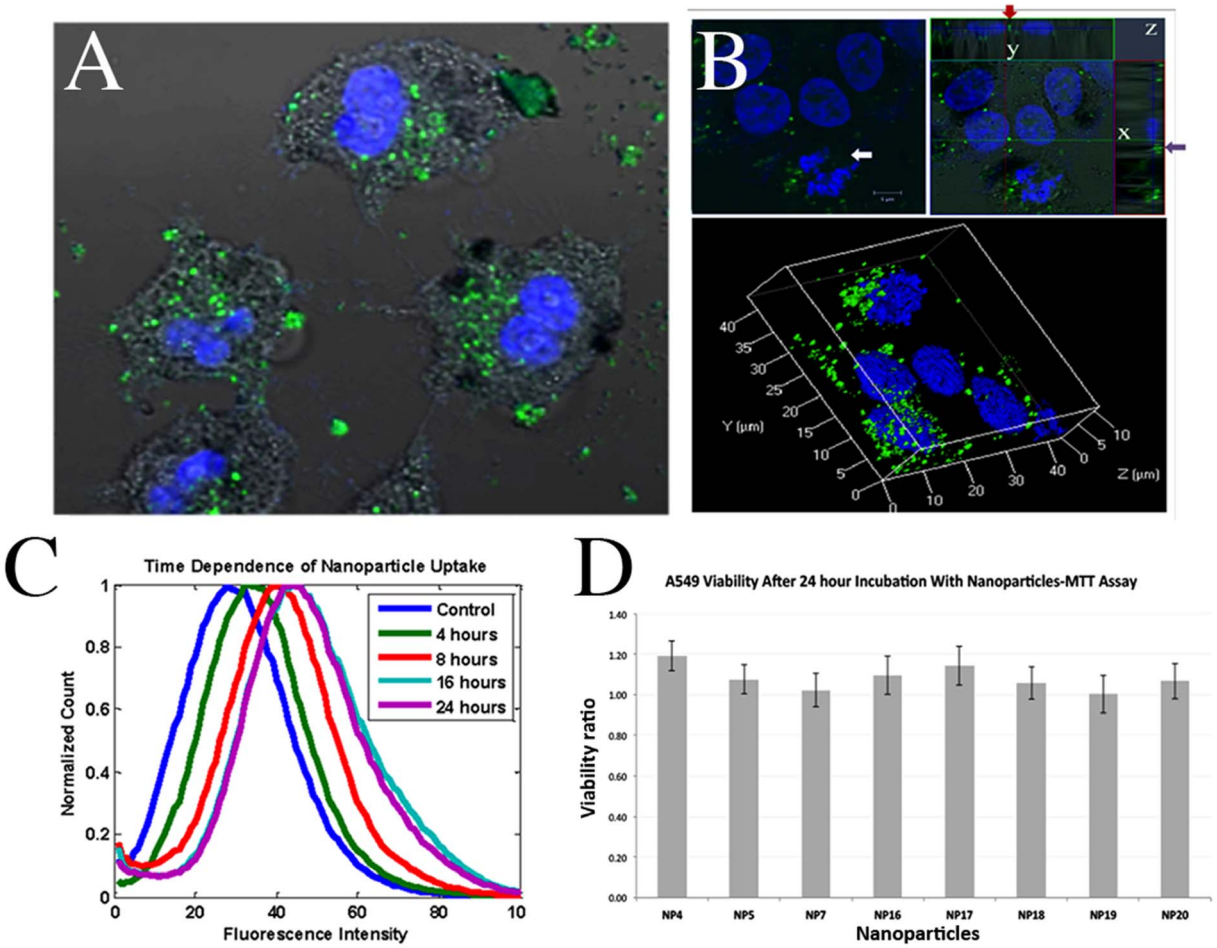

Fig. 4 Nanoparticle uptake by A549 cells. (A) and (B) DIC image and fluorescence images of A549 cells incubated with FITC-C-NPs. FITC-C-NPs appear green in the fluorescence images and as dark regions in the DIC image. Note the heterogeneity in nanoparticle localization. The slices are obtained by acquiring confocal images and show NPs within the cytoplasmic volume of some cells. Hoechst is used as nuclear stain. (C) The histograms shows fluorescence intensity measured *via* flow cytometry of different time points after treating A549 cells with FITC-C-NPs. Maximum uptake is seen after 16 hours. (D) MTT assay for the viability of A459 cells incubated with NPs.

well chamber was covered with aluminum foil and one was kept uncovered. The 8-well chambers were excited with white light for 15 min. Following excitation, the 8-well chamber was imaged and then placed in a humidified CO_2 incubator. After 16 h of incubation, calcein-AM was added to each well and images were obtained. Calcein-AM is a permeable dye that enters the cells where endogenous esterases cleave the AM group rendering the now fluorescent calcein impermeable. Living cells retain the dye within the cytoplasm while dead cells lose the dye. Fluorescence microscopy and differential interference contrast (DIC) imaging were performed and living cells were counted in an automated way using Cell Profiler software while dead cells were counted manually by looking for cells that had lost the calcein fluorescence.

Cellular uptake

We assessed the uptake of NPs into A549 cells using two independent methods: flow cytometry and microscopy. In flow cytometry experiments, we quantified the uptake of fluorescein isothiocyanate (FITC) labeled C-NPs (FITC-C-NPs) by cells. Cells were seeded in 6 well plates (10^4 cells per cm^2) until reaching 50% confluence after which FITC-C-NPs were added. At different time points, cells were washed, trypsinized, and collected by centrifugation at 100*g* and re-suspended in 4% formaldehyde with a gentle vortexing to avoid cell clumping. Cell suspensions were analyzed by flow cytometry where fluorescence intensity was plotted for each sample.

Nanoparticles internalization was assessed by confocal microscopy. A549 cells were seeded in confocal dishes and loaded with FITC-C-NPs overnight. Right before imaging, a blue fluorescent cell marker dye (calcein-blue AM) was added. After thorough washing of the un-internalized dye, z-stacks and reconstitution images of the cells were acquired.

Measurement of intracellular ROS

Intracellular ROS generation was assessed in A549 D-NPs-loaded cells by an ROS sensitive dye, dihydroethidium (DHE). Dihydroethidium was used according to the manufacturer's protocol. Cells were cultured in confocal dishes, loaded with D-NPs overnight, washed with PBS and incubated with 3 μM DHE at 37 °C for 15 min. Cells were then excited for 5 min and live imaged at 520 nm.

Results and discussion

Core–shell–shell magnetite–silica–titania nanoparticles (Fe_3O_4@SiO_2@TiO_2 NPs) (C-NPs), Scheme 1, were prepared by successive sol–gel methods. SEM, Fig. 1, characterized the morphology of the various nanocomposites. The FTIR, XRD and

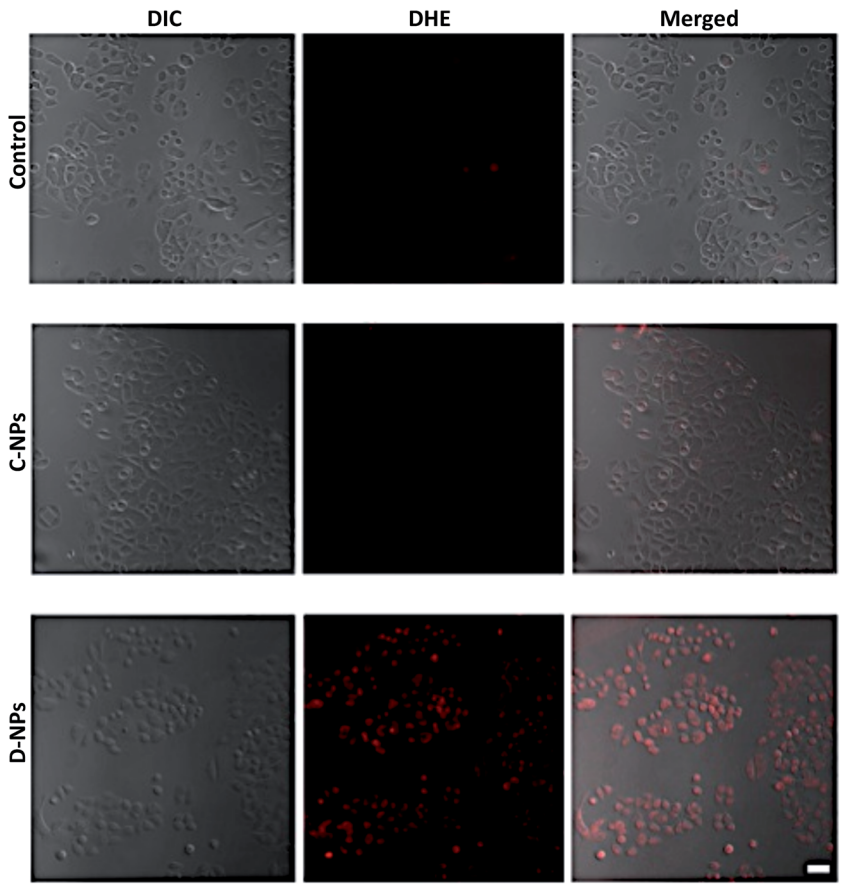

Fig. 5 Differential interference contrast (DIC) images (left), ethidium fluorescence (DHE, middle) and merged images of both DIC and DHE (right) of A549 excited cells. ROS production is significantly increased in D-NPs loaded cells. C-NPs loaded cells and unloaded cells have very low levels of ROS. Scale bar: 5 μm.

particle size distributions obtained from SEM images of the different samples are provided in the ESI, Fig. S1 to S3,† and the mean equivalent diameters of the samples are summarized in Table 1.

The hydrodynamic diameter of the different nanocomposites was measured using DLS (see ESI, Fig. S4†). The mean hydrodynamic diameter increased from 62 nm for A-NPs to 90 nm for B-NPs, and 99 nm for C-NPs, which is within the optimum size range for cellular uptake.[57]

The total ROS generation in solution upon light irradiation was measured using DCFH as a probe. The latter is a non-fluorescent molecule, however, in the presence of ROS in solution, it's readily oxidized to DCF which is highly fluorescent.[58] The emission fluorescence intensity at 520 nm of several samples (Blank, A-NPs, B-NPs, C-NPs, D-NPs, dye, and Degussa P25 TiO_2 NPs) was measured at successive excitation with 532 nm monochromatic light, Fig. 2, and white light (ESI, Fig. S5†). The results of A-NPs and B-NPs were comparable to the blank/control trials. Degussa P25 TiO_2 NPs generated slightly higher fluorescence intensities than the control. ROS generated by dye and C-NPs showed similar effectiveness in oxidizing DCFH, however, neither of which achieved what D-NPs were able to. After the first excitation, which lasted for 5 min, the NPs were left in the dark for 5 min and then were excited again for

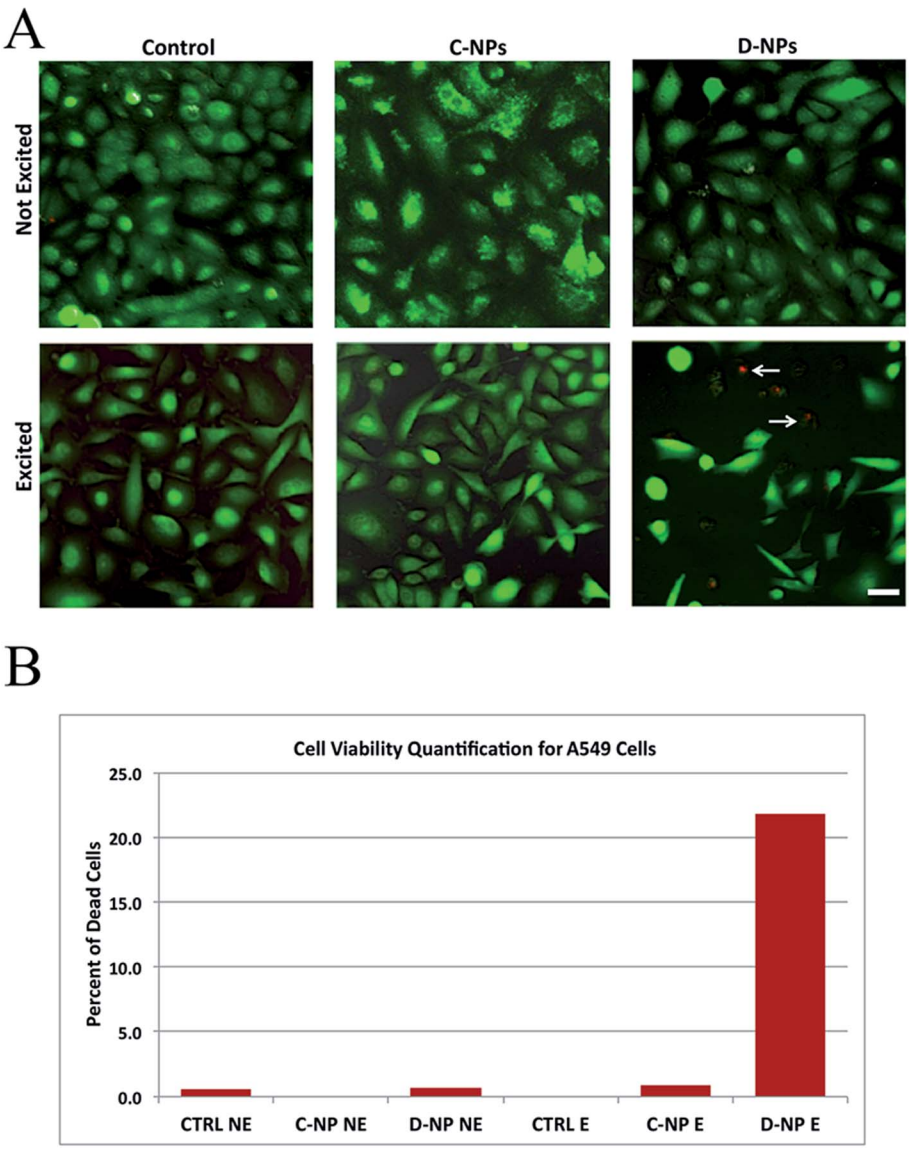

Fig. 6 Excitation of A549 D-NPs loaded cells with a white light source induces cell death. (A) Images of excited (E) and non-excited (NE) A549 D-NPs loaded cells and unloaded cells were taken 16 hours after excitation. C-NPs loaded cells and unloaded cells were used as controls. Images were captured with 488 nm and 561 nm channels representing calcein and PI stain, respectively. The red spots indicate dead cells that took up the PI stain in excited D-NPs loaded cells. The total number of cells is less and most of the dead cells were washed out. Scale bar: 10 μm. (B) Quantification of cell viability by counting the number of living (calcein green containing) and dead cells (non-calcein green containing). Significant numbers of dead cells were observed only with excitation of D-NPs. Control (CTRL) are non-loaded cells. NE and E refer to not excited and excited, respectively.

another 5 min. The further increase in DCF fluorescence intensity indicates that more ROS has been generated following every excitation (a similar trend was observed after 2 more excitations, but data are not shown). After 2 excitations only, D-NPs generated more than 5 times with green light, and around 4 times with white light, what any of the other samples were able to. This suggests that the quantity of ROS generated can be controlled by the frequency of excitations.

In the second set of experiments, we chose a singlet-oxygen-specific molecular probe (9,10-dimethylanthracene, DMA) to measure if any $^1O_2$ is generated by D-NPs. DMA is a fluorescent compound ($\lambda_{ex} = 375$ nm, $\lambda_{em} = 436$ nm) that reacts selectively with $^1O_2$ to form the non-fluorescent 9,10-endoperoxide with a very high rate constant (2×10^7 to 9×10^8 M^{-1} s^{-1}) in many organic solvents, as well as in water.[58] The endo-peroxide generation was measured using two different spectroscopic methods: UV-Vis and fluorescence. Fig. 3 shows the UV-Vis spectra of D-NPs along with those of dye and a control/blank before and after excitation with 532 nm light. DMA absorbance at 375 nm decreased from 0.89 to 0.53 (more than 40%) in 80 min of illumination. In contrast, the D-NPs and the blank/control showed practically no decrease in DMA absorbance confirming the absence of any singlet oxygen generation. The fluorescence spectra, Fig. 3, show a similar result. Dye was able to generate enough singlet oxygen in 80 min to decrease the fluorescence intensity of DMA at 424 nm by more than 35%. The spectra of D-NPs and the blank are similar and show negligible decrease in fluorescence after 80 min of excitation, a result that echoes the UV-Vis findings.

After demonstrating the efficiency of D-NPs at generating ROS in solution, we set to assess their efficacy at killing malignant cells upon light excitation. We chose A549 cells, a commonly used lung cancer cell line model, to determine their NPs internalization, in-cell ROS generation and light induced cell death.

The uptake of NPs into A549 cells was assessed using two independent methods: flow cytometry and fluorescence microscopy. In the former, we quantified the uptake of fluorescein isothiocyanate (FITC) labeled C-NPs (FITC-C-NPs) by cells. This enabled us to use fluorescence assays to measure nanoparticle uptake and visualize nanoparticles within cells. As shown in Fig. 4A, A549 cells incubated with FITC-C-NPs take up the NPs over several hours with no increase in uptake after 16 hours (Fig. 1C), and therefore all subsequent experiments were performed after at least 16 hours of incubation time.

However, flow cytometry, while excellent at quantifying overall fluorescence associated with cells, it does not assert whether the NPs are indeed internalized into the cells. Therefore, laser scanning confocal microscopy was performed to ensure the internalization (Fig. 4B). The internalization of the NPs into cells is ensured using z-stack optical sectioning and reconstructed 3D image using confocal microscopy (Fig. 4B), which demonstrates that the NPs are within the cytoplasmic volume of the cells. We also observed that some nanoparticles appear to be at the periphery of the cells, which could be either at the cell membrane or just within it. The viability of cells loaded with different batches of NPs (without excitation) was determined by the MTT assay (Fig. 4D). The results show that the cells proliferate normally in Fig. 4D and visually in Fig. 4B (dividing cells, white arrow). The IC_{50} value calculated from the percentage of viability of excited cells loaded with different concentrations of NPs is 3 μg ml^{-1}.

ROS production was assessed using a DHE oxidation assay (Fig. 5). DHE is a cell-permeable dye that is oxidized by superoxide anions, leading to the formation of red fluorescent dye (ethidium) that intercalates with nuclear DNA. The fluorescence intensity of the ethidium corresponds to the amount of superoxide produced in the cells. D-NPs loaded cells, control unloaded cells and control C-NPs loaded cells were incubated with DHE, excited and directly imaged. A significant increase in ROS

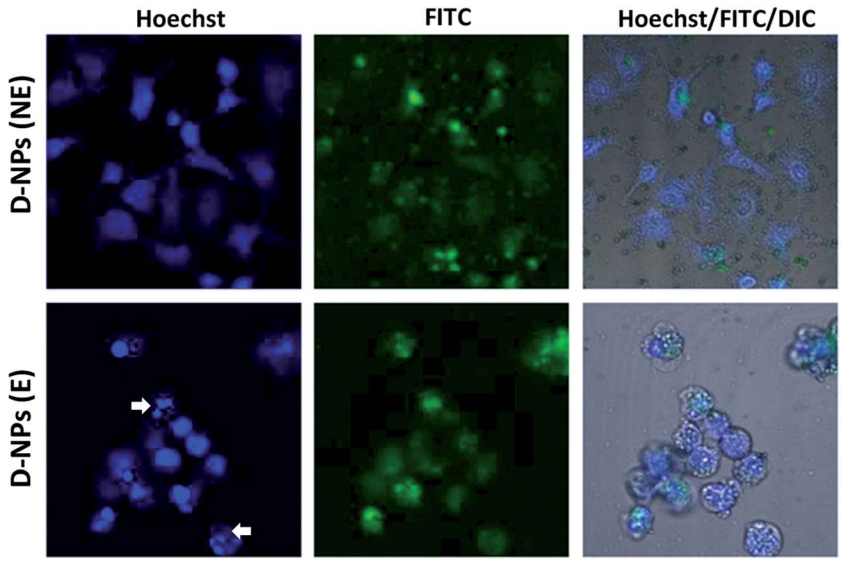

Fig. 7 Excitation of A549 D-NPs loaded cells induces apoptosis, indicated by white arrows. NE and E refer to not excited and excited, respectively. Hoechst is used as nuclear stain.

production was observed in D-NPs cells as compared to the basal level produced in control cells.

The observation that D-NPs loaded cells showed large ROS production within cells following excitation suggested that the viability would be compromised. To test this we carried out a microscopy based viability assay. Control unloaded cells, control C-NPs loaded cells and D-NPs loaded cells were all excited with white light (UV filter < 350 nm) for 15 min. After 24 hours calcein-AM was added to assess by imaging the viability of the cells. Living cells with intact cell membranes retain calcein while dead cells lose the dye. Excited D-NPs loaded cells show a large increase in cell death as compared to control cells or to cells loaded with C-NPs (Fig. 6). In control cells and in non-excited cells, cell death was less than 1% of all cells while in excited D-NPs loaded cells it was 20 to 40% of all cells. Furthermore, while our experiment showed a large increase in cell death compared to controls, this increase ranged from 20–40% of all cells. It is possible that this is due to the fact that different cells took up different amounts of nanoparticles as shown in Fig. 4B, and/or different cells may also have varying ROS scavenging systems.

Finally, we demonstrate the induction of tumoricidal activity of the ROS where cells loaded with NPs either excited (Fig. 7, lower set) or left unexcited (Fig. 7, top set) reveal a potent cell death activity in the excited cells. Based on Hoechst stain, we recognize apoptotic nuclei and fragments (white arrow heads). Although no attempt was made to investigate the mode of cell death, it is well established that ROS induces apoptosis in several cell types. Irrespective of the mode of cell death, the tumoricidal action of these NPs is clearly demonstrated.

Conclusion

In this work, we report the preparation of core–shell–shell magnetite–silica–titania nanoparticles (Fe_3O_4@SiO_2@TiO_2 NPs), which were stained with a polypyridyl ruthenium dye. The dyed NPs (D-NPs) proved superior to both the naked NPs and the dye alone at generating ROS in solution upon excitation with either white or green light. However, in the ROS generated in solution by the D-NPs no detection of $^1O_2$ was found. We further demonstrated in a proof-of-concept experiment that these nanoparticles are taken up by A549 lung cancer cells. Excitation of these D-NPs loaded A549 cells show an intracellular increase in ROS, and a large increase in cell death after 24 h. The mechanism of cell death induction is currently under investigation. Previous studies have shown a link between ROS generation and apoptosis induction. For cancer treatment an apoptotic cell death is preferred as this is a regulated process with macrophages, which are able to take up the apoptotic cells. Necrosis on the other hand results in the release of cell contents into the medium, which can result in greater inflammation. Determining the mechanism of cell death induction with our nanoparticles is therefore an important aim of our future work. It would be also interesting to determine if different levels of oxygen affect the cell death mechanism. The advantage of the D-NPs might be in its efficient action against low-oxygen cancerous cells.

Acknowledgements

The Lebanese National Council for Scientific Research (CNRS), University Research Board (URB), Farouk Jabr grant, and Medical Practice Plan (MPP) funds at the American University of Beirut.

References

1 T. Nann, *Nano Biomed. Eng.*, 2011, **3**, 137–143.
2 W.-T. Li, *Nanoparticles for photodynamic therapy*, Wiley-VCH Verlag GmbH & Co. KGaA, 2011.
3 S. A. Sibani, P. A. McCarron, A. D. Woolfson and R. F. Donnelly, *Expert Opin. Drug Delivery*, 2008, **5**, 1241–1254.
4 R. R. Allison, G. H. Downie, R. Cuenca, X.-H. Hu, C. J. H. Childs and C. H. Sibata, *Photodiagn. Photodyn. Ther.*, 2004, **1**, 27–42.
5 D. Bechet, P. Couleaud, C. Frochot, M.-L. Viriot, F. Guillemin and M. Barberi-Heyob, *Trends Biotechnol.*, 2008, **26**, 612–621.
6 A. A. Abdel-Shafi, P. D. Beer, R. J. Mortimer and F. Wilkinson, *Phys. Chem. Chem. Phys.*, 2000, **2**, 3137–3144.
7 G. Lemercier, A. Bonne, M. Four and L. M. Lawson-Daku, *C. R. Chim.*, 2008, **11**, 709–715.
8 S. C. Boca, M. Four, A. Bonne, B. van der Sanden, S. Astilean, P. L. Baldeck and G. Lemercier, *Chem. Commun.*, 2009, 4590–4592.
9 C. Mari, V. Pierroz, R. Rubbiani, M. Patra, J. Hess, B. Spingler, L. Oehninger, J. Schur, I. Ott, L. Salassa, S. Ferrari and G. Gasser, *Chem. –Eur. J.*, 2014, **20**, 14421–14436.
10 E. Wachter, D. K. Heidary, B. S. Howerton, S. Parkin and E. C. Glazer, *Chem. Commun.*, 2012, **48**, 9649–9651.
11 C. T. Poon, P. S. Chan, C. Man, F. L. Jiang, R. N. Wong, N. K. Mak, D. W. Kwong, S. W. Tsao and W. K. Wong, *J. Inorg. Biochem.*, 2010, **104**, 62–70.
12 J.-X. Zhang, J.-W. Zhou, C.-F. Chan, T. C.-K. Lau, D. W. J. Kwong, H.-L. Tam, N.-K. Mak, K.-L. Wong and W.-K. Wong, *Bioconjugate Chem.*, 2012, **23**, 1623–1638.
13 S. Rani-Beeram, K. Meyer, A. McCrate, Y. Hong, M. Nielsen and S. Swavey, *Inorg. Chem.*, 2008, **47**, 11278–11283.
14 K. Davia, D. King, Y. Hong and S. Swavey, *Inorg. Chem. Commun.*, 2008, **11**, 584–586.
15 F. Schmitt, P. Govindaswamy, G. Süss-Fink, W. H. Ang, P. J. Dyson, L. Juillerat-Jeanneret and B. Therrien, *J. Med. Chem.*, 2008, **51**, 1811–1816.
16 T. Gianferrara, A. Bergamo, I. Bratsos, B. Milani, C. Spagnul, G. Sava and E. Alessio, *J. Med. Chem.*, 2010, **53**, 4678–4690.
17 J. Onuki, A. V. Ribas, M. H. G. Medeiros, K. Araki, H. E. Toma, L. H. Catalani and P. Di Mascio, *Photochem. Photobiol.*, 1996, **63**, 272–277.
18 M. Narra, P. Elliott and S. Swavey, *Inorg. Chim. Acta*, 2006, **359**, 2256–2262.
19 H. Ke, W. Ma, H. Wang, G. Cheng, H. Yuan, W.-K. Wong, D. W. J. Kwong, H.-L. Tam, K.-W. Cheah, C.-F. Chan and K.-L. Wong, *J. Lumin.*, 2014, **154**, 356–361.

20 M. Pernot, T. Bastogne, N. P. E. Barry, B. Therrien, G. Koellensperger, S. Hann, V. Reshetov and M. Barberi-Heyob, *J. Photochem. Photobiol., B*, 2012, **117**, 80–89.
21 J. X. Zhang, K.-L. Wong, W.-K. Wong, N.-K. Mak, D. W. J. Kwong and H.-L. Tam, *Org. Biomol. Chem.*, 2011, **9**, 6004–6010.
22 R. Lincoln, L. Kohler, S. Monro, H. Yin, M. Stephenson, R. Zong, A. Chouai, C. Dorsey, R. Hennigar, R. P. Thummel and S. A. McFarland, *J. Am. Chem. Soc.*, 2013, **135**, 17161–17175.
23 A. Frei, R. Rubbiani, S. Tubafard, O. Blacque, P. Anstaett, A. Felgenträger, T. Maisch, L. Spiccia and G. Gasser, *J. Med. Chem.*, 2014, **57**, 7280–7292.
24 Z. Huang, H. Xu, A. D. Meyers, A. I. Musani, L. Wang, R. Tagg, A. B. Barqawi and Y. K. Chen, *Technol. Cancer Res. Treat.*, 2008, **7**, 309–320.
25 Q. Chen, Z. Huang, H. Chen, H. Shapiro, J. Beckers and F. W. Hetzel, *Photochem. Photobiol.*, 2002, **76**, 197–203.
26 W.-D. Jang and H.-J. Yoon, *J. Porphyrins Phthalocyanines*, 2013, **17**, 16–26.
27 X. Feng, S. Zhang and X. Lou, *Colloids Surf., B*, 2013, **107**, 220–226.
28 A. O. Fujishima, J. Ohtsuki, T. Yamashita and S. Hayakawa, *J. Photomed. Photobiol.*, 1986, 45–46.
29 M. Xu, J. Ma, J. Gu and Z. Lu, *Supramol. Sci.*, 1998, **5**, 511–513.
30 K. Hirakawa, M. Mori, M. Yoshida, S. Oikawa and S. Kawanishi, *Free Radical Res.*, 2004, **38**, 439–447.
31 T. Ashikaga, M. Wada, H. Kobayashi, M. Mori, Y. Katsumura, H. Fukui, S. Kato, M. Yamaguchi and T. Takamatsu, *Mutat. Res., Genet. Toxicol. Environ. Mutagen.*, 2000, **466**, 1–7.
32 S. Zhang, D. Yang, D. Jing, H. Liu, L. Liu, Y. Jia, M. Gao, L. Guo and Z. Huo, *Nano Res.*, 2014, **7**, 1659–1669.
33 S.-S. Song, B.-Y. Xia, J. Chen, J. Yang, X. Shen, S.-J. Fan, M.-l. Guo, Y.-M. Sun and X.-D. Zhang, *RSC Adv.*, 2014, **4**, 42598–42603.
34 N. Miyoshi, K. Kume, K. Tsutumi, Y. Fukunaga, S. Ito, Y. Imamura and A. B. Bibin, *AIP Conf. Proc.*, 2011, **1415**, 21–23.
35 Y. Kubota, M. Hosaka, K. Hashimoto and A. Fujishima, *Gaodeng Xuexiao Huaxue Xuebao*, 1995, **16**, 56–62.
36 L. Chen, J.-w. Xiong, G.-x. Liu and Z.-x. Zhang, *Guangdianzi, Jiguang*, 2007, **18**, 1265–1268.
37 X. Feng, S. Zhang, H. Wu and X. Lou, *Colloids Surf., B*, 2015, **125**, 197–205.
38 Z. Hu, Y. Huang, S. Sun, W. Guan, Y. Yao, P. Tang and C. Li, *Carbon*, 2012, **50**, 994–1004.
39 S. Yamaguchi, H. Kobayashi, T. Narita, K. Kanehira, S. Sonezaki, Y. Kubota, S. Terasaka and Y. Iwasaki, *Photochem. Photobiol.*, 2010, **86**, 964–971.
40 H. Zhang, R. Shi, A. Xie, J. Li, L. Chen, P. Chen, S. Li, F. Huang and Y. Shen, *ACS Appl. Mater. Interfaces*, 2013, **5**, 12317–12322.
41 A. Sette, J. Spadavecchia, J. Landoulsi, S. Casale, B. Haye, O. Crociani and A. Arcangeli, *J. Nanopart. Res.*, 2013, **15**, 2111.
42 J. Xu, Y. Sun, J. Huang, C. Chen, G. Liu, Y. Jiang, Y. Zhao and Z. Jiang, *Bioelectrochemistry*, 2007, **71**, 217–222.
43 L. Chen, M.-x. Liao and J.-w. Xiong, *Guangdianzi, Jiguang*, 2008, **19**, 278–281.
44 K. Huang, L. Chen, J. Deng and J. Xiong, *J. Nanomater.*, 2012, 720491.
45 Z. Li, L. Mi, P.-N. Wang and J.-Y. Chen, *Nanoscale Res. Lett.*, 2011, **6**, 356–357.
46 Y. Xiong, C. Liang, H. Xiao and J. Xiong, *Adv. Mater. Res.*, 2011, **152–153**, 136–143.
47 K. Pathakoti, S. Morrow, C. Han, M. Pelaez, X. He, D. D. Dionysiou and H.-M. Hwang, *Environ. Sci. Technol.*, 2013, **47**, 9988–9996.
48 M. Liao, H. He and J. Xiong, *Jiguang Shengwu Xuebao*, 2009, **18**, 324–328.
49 Z. Li, X. Pan, T. Wang, P.-N. Wang, J.-Y. Chen and L. Mi, *Nanoscale Res. Lett.*, 2013, **8**, 91–97.
50 Y. Tokuoka, M. Yamada, N. Kawashima and T. Miyasaka, *Chem. Lett.*, 2006, **35**, 496–497.
51 J. Spadavecchia, C. Methivier, J. Landoulsi and C.-M. Pradier, *ChemPhysChem*, 2013, **14**, 2462–2469.
52 T. Lopez, E. Ortiz, M. Alvarez, J. Navarrete, J. A. Odriozola, F. Martinez-Ortega, E. A. Páez-Mozo, P. Escobar, K. A. Espinoza and I. A. Rivero, *Nanomed. Nanotechnol. Biol. Med.*, 2010, **6**, 777–785.
53 W. Lei, Q. Zhou, Z. Li, X. Wang and B. Zhang, *Chem. Lett.*, 2009, **38**, 1138–1139.
54 A. Janczyk, A. Wolnicka-Glubisz, K. Urbanska, G. Stochel and W. Macyk, *J. Photochem. Photobiol., B*, 2008, **92**, 54–58.
55 Y. Ding, K. Song, X. Gu, J. Zhou and Y. Feng, *Nanjing Shida Xuebao, Ziran Kexueban*, 2009, **32**, 79–82.
56 S. C. Pang, S. Y. Kho and S. F. Chin, *J. Nanomater.*, 2012, 427310–427316.
57 Wahajuddin and S. Arora, *Int. J. Nanomed.*, 2012, **7**, 3445–3471.
58 A. Gomes, E. Fernandes and J. L. F. C. Lima, *J. Biochem. Biophys. Methods*, 2005, **65**, 45–80.